Photodissociation dynamics of acetone at 193 nm: Photofragment internal and translational energy distributions

Karen A. Trentelman,[a] Scott H. Kable, David B. Moss,[b] and Paul L. Houston
Department of Chemistry, Baker Laboratory, Cornell University, Ithaca, New York 14853-1301

(Received 19 June 1989; accepted 8 September 1989)

The photofragment internal and translational energy distributions resulting from the 193 nm photolysis of acetone have been measured. Vacuum-ultraviolet laser-induced fluorescence was used to probe the CO fragment, and multiphoton ionization time-of-flight mass spectrometry was used to probe the CH_3. A Boltzmann distribution was observed to fit each degree of freedom with the following characteristic temperatures: CO: $T_{vib} = 2700$ K, $T_{rot} = 3000$ K, $T_{trans} = 3000$ K; CH_3: $T_{vib} = 800$ K, $T_{rot} = 500$ K, $T_{trans} = 3500$ K. No evidence was found for two distinct CH_3 populations, as might be characteristic of a stepwise reaction. Energy partitioning between the fragments was fit well by a simple impulsive model in which the available energy is divided equally between the two dissociating C–C bonds, the two bonds cleaving in rapid succession on a time scale short enough to allow little redistribution of energy into the methyl degrees of freedom.

I. INTRODUCTION

As the simplest ketone, acetone has long been used as a prototype for studies of photophysics and photochemistry of this important class of molecules. Much of the photochemical research from the prelaser era was summarized in the review of Lee and Lewis.[1] These early experiments indicated that the primary photochemical event is the cleavage of one or both C–C bonds, producing one or two methyl radicals in coincidence with acetyl radical or CO, respectively.

Subsequent studies have clarified the picture considerably. Excitation via the $\pi^* \leftarrow n$ transition to the S_1 state results in cleavage of a single C–C bond to produce methyl and acetyl radicals. The measurements of photofragment translation by Hancock and Wilson[2] following excitation at 266 nm indicated that roughly 40% of the 130 kJ/mol excess energy in this system is partitioned into fragment translation, leaving approximately 80 kJ/mol (> 6000 cm^{-1}) as fragment internal excitation. When shorter wavelengths (< 200 nm) are used to excite the $3s \leftarrow n$ Rydberg transition, both C–C bonds are broken, producing CO and two methyl radicals with near unit quantum yield.[3,4]

Such a three-body dissociation is a complicated theoretical problem and presents several intriguing questions whose answers may be obtained experimentally. Of particular interest is the sequence of events that takes place on the excited potential surface(s). Does the dissociation proceed directly on the initially excited surface, or does the system predissociate, crossing from a quasi-bound surface to a lower unbound surface? What molecular motions are coupled to the reaction coordinate? What is the structure of the transition state? Do the two C–C bonds rupture sequentially, or simultaneously in a concerted process? Several recent studies have addressed these issues for the $3s \leftarrow n$ Rydberg state of acetone, and their conclusions are summarized briefly here.

Baba *et al.*[5] measured the yield of acetone fragment ions following multiphoton excitation by an ArF excimer laser at 193 nm. The power dependence of the acetyl ion signal ($m/e = 43$) suggested that the ion was produced as a result of absorption of the laser radiation by a relatively long-lived neutral acetyl fragment, rather than via decomposition of a metastable parent ion. They took this result as evidence of a sequential bond rupture mechanism.

Vaida and co-workers[6,7] have recently measured the $3s \leftarrow n$ absorption spectrum of acetone in a supersonic jet and noted the effects of increased clustering on the spectrum. In their model, changes in the vibronic structure of the absorption spectrum reflect changes in the coupling of a vibrational coordinate to the dissociation channel caused by cluster formation. They observed that vibrations ν_{16} (out-of-plane skeletal bend), ν_8 (C–C–O bend), and ν_4 and ν_5 (methyl umbrella motions) are more active in the cluster spectrum than in the monomer, suggesting that they are important to the dissociation. Activity in the umbrella motion is expected, since the tetrahedral bound methyls must transform to planar free methyls. ν_8 and ν_{16} are believed to promote coupling between the $3s \leftarrow n$ state (S_2) and the coupled $\{S_1, T_1\}$ $\pi^* \leftarrow n$ surfaces, indicating a predissociative mechanism. This is also consistent with their observations of resolved vibronic structure in the $3s \leftarrow n$ spectrum, characteristic of a quasi-bound state rather than a purely dissociative one.

One of the most important pieces of information in photodissociation dynamics is the nascent distribution of internal energy in the fragments. Leone and co-workers[8,9] have performed a series of experiments on the products of acetone photolyzed at 193 nm. All of the experiments made use of time- and energy-resolved infrared fluorescence from vibrationally excited photoproducts, CO and CH_3. The first experiments of Donaldson and Leone[8] used a circular variable filter with a bandpass of 30–60 cm^{-1} to resolve the emission.

[a] Present address: Department of Chemistry, Northwestern University, Evanston, IL 60208.
[b] Present address: Department of Physics, Lynchburg College, Lynchburg, VA 24501.

 0021-9606/89/247498-16$02.10

The observed rovibrational band contours were fit to vibrational and rotational distributions for the CO stretch and the CH_3 antisymmetric stretch (ν_3). The CO vibrational distribution for $v = 1$–3 fit a temperature of ~ 1200 K, while the rotational distribution (during approximately the first μs) was highly excited, peaking in the vicinity of $J = 32$, but was not fit well by a single temperature. Rapid vibrational relaxation interfered with the measurement of the methyl ν_3 distribution, but the results were consistent with a rotational temperature of ~ 1500 K and a ratio of $v_3 = 1/2/3$ of 0.73/0.14/0.13.

The more recent experiments of Woodbridge *et al.*[9] used a Fourier transform spectrometer to detect the IR emission with $\leqslant 1$ cm^{-1} resolution. With this apparatus they were able to resolve more fully the rovibrational structure of the CO stretching band and thus obtain a more accurate measurement of the nascent rotational and vibrational distribution in the CO fragment. They determined an approximate vibrational temperature of 2000 K based on emission from several fully resolved rotational lines in each of $v = 1$–3. They were also able to fit the rovibrational structure in the P branch of $v = 1$ and both P and R branches of $v = 2,3$ to a rotational temperature of ~ 3400 K, under conditions they believed to allow no more than one hard-sphere collision per CO.

All of these results are consistent with the mechanism outlined above, namely a predissociation with sequential breaking of the two C–C bonds, the second bond rupture occurring after an undetermined delay and imparting a forceful rotational "kick" to the departing CO. Nevertheless, there are some issues that remain to be addressed. In particular, measurement of the photofragment translational energies would not only reveal linear momentum constraints on the dynamics, but would also be beneficial in determining whether the bulb experiments are as collision-free as expected. In addition, the population distribution in all of the methyl vibrations, particularly the umbrella motion ν_2 has yet to be determined. If the two methyl radicals have distinguishable internal or translational energy distributions, that information might reveal something about the intramolecular vibrational dynamics prior to and during the dissociation. A direct measurement of the CO ground vibrational state population could verify that it is in fact the most populous and is fit by the same rotational and vibrational temperatures observed for the vibrationally excited states. Finally, comparing the overall partitioning of vibrational, translational and rotational energy to model predictions may help determine the relative time scale for breaking the two C–C bonds.

In this work, we attempt to address some of these issues. We have measured the internal and translational energy distributions of both the CO and CH_3 fragments produced by acetone photolysis at 193 nm. The experimental results constitute a measurement of the energy distributions in *all* of the fragment degrees of freedom. These are compared with the predictions of simple models of the photodissociation and the results of previous experiments to yield a detailed description of the dissociation dynamics.

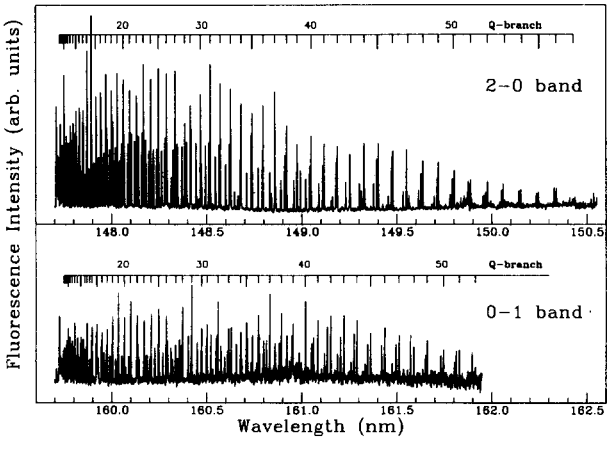

FIG. 1. VUV-LIF spectra of the CO photofragment following 193 nm dissociation of acetone. (a) $v'' = 0$ from the 2–0 band; (b) $v'' = 1$ from the 0–1 band. (Note that the rotational distribution in $v'' = 1$ appears to peak at higher J than in $v'' = 0$.)

II. EXPERIMENTAL

Several experimental techniques were utilized to probe the internal state distributions of the acetone photofragments. CO was probed via vacuum ultraviolet laser-induced fluorescent (VUV-LIF) and Doppler profiles of individual rotational lines were measured to determine the translational energy distribution. The internal energy distribution of methyl was probed via $2 + 1$ multiphoton ionization (MPI) with mass resolved time-of-flight (TOF) detection. The fragment recoil velocity was measured using the pulsed extraction field technique. All of these techniques and the apparatus used for this study have been described in other publications.[10,11] Some relevant details are discussed below.

The sample was prepared by expanding room temperature acetone (Fisher Scientific) in helium through a 500 μm orifice at a total stagnation pressure of 200–250 kPa (2–2.5 atm) resulting in an expansion of 11%–15% acetone in helium. The acetone was subjected to at least one freeze–pump–thaw cycle in order to remove gaseous impurities. The beam valve was operated at 10 Hz with an open pulse duration of approximately 200 μs. The photolysis laser for all experiments was an ArF excimer (40–50 mJ/pulse at 193 nm), softly focused into the interaction region.

For the VUV-LIF experiments, the sample was an uncollimated free jet expansion, the interaction region typically 20–30 nozzle diameters downstream from the source. The CO fragment was probed 200 ns following the photolysis using tunable VUV radiation in the range from 140 to 170 nm generated by four-wave sum frequency mixing of two visible dye lasers in magnesium vapor.[10] The first dye laser (ω_1) is tuned to a two-photon resonance in the magnesium, while the other (ω_2) is tuned through an autoionizing continuum. The laser-induced fluorescence was collected with a solar blind PMT fitted with a 193 nm filter, processed in a gated integrator boxcar averager, digitized, and recorded by

a computer acquisition system that also controlled the scan of the tunable VUV.

For Doppler profile measurements, intracavity etalons in both dye lasers were used to narrow the VUV linewidth to approximately 0.21 cm^{-1}. Computer-controlled pressure tuning of ω_2 was used to scan the VUV radiation across a single v'',J'' line.

The effect on our data of clusters in the supersonic expansion was investigated by utilizing the cluster-free environment afforded by an effusive beam. To create such an environment, an adapter was constructed for the pulsed valve which allows the cooled expansion to be collisionally rethermalized. This provided what is effectively a pulsed effusive beam source. A VUV-LIF spectrum of dilute CO (0.03%) in He taken in the effusive beam was indistinguishable from that obtained in a room temperature static bulb sample of CO, confirming that the adapter indeed completely rethermalizes the expanded sample. The conditions of these effusive beam experiments are identical to the supersonic beam experiment in all other respects. This setup has the advantage of providing a thermal sample without the problems of sample depletion and attenuation of the VUV which would be present in a static bulb experiment.

For the MPI-TOF experiments, the free jet expansion was collimated with two 1 mm diameter skimmers, producing a molecular beam less than 2 mm in diameter in the differentially pumped chamber used for mass spectrometry, roughly 1 m from the beam source. The methyl fragment internal state distribution was probed via 2 + 1 MPI using a frequency doubled Nd:YAG pumped dye laser system in the range from 315–340 nm. The ions were mass selected in a TOF mass spectrometer, detected with a particle multiplier, preamplified (10×), and then processed in the same manner as the CO fluorescence signal.

For the pulsed field experiments, the mass spectrometer was operated without the usual DC acceleration field. The extraction field was produced by a high voltage pulse generator at a variable delay following the photolysis. The amplitude of the field could be adjusted from 0–2000 V and the duration of the pulse was 2 μs. The amplified ion signal was digitized and averaged with a digital storage oscilloscope and subsequently transferred to a computer for storage and analysis.

III. RESULTS

A. CO fragment internal energy

The distribution of energy among the internal degrees of freedom of the nascent CO fragment was determined by the method of vibrationally and rotationally resolved vacuum ultraviolet laser induced fluorescence (VUV-LIF) excitation spectroscopy. CO molecules were electronically excited through the $A\,^1\Pi \leftarrow X\,^1\Sigma^+$ transition by tunable VUV radiation. The subsequent $A \rightarrow X$ fluorescence was monitored as a function of the excitation laser wavelength.

LIF spectra obtained for $v'' = 0$ and 1 are presented in Fig. 1. The spectra display a great deal of rotational excitation. We observe population from $J'' = 0$ to > 60 (peaking near $J'' = 22$) in $v'' = 0$ and $J'' = 0$ to > 55 (peaking near $J'' = 27$) in $v'' = 1$. In $v'' = 2$ (not shown) we observe population from $J'' = 0$ to > 30. The signal-to-noise decreases with increasing v'', limiting the amount of available data from $v'' = 2$ and prohibiting investigation of $v'' = 3$ by this technique.

1. Rotational distributions

a. Spectroscopic considerations. Rotational levels of the CO $A\,^1\Pi$ state, especially those in $v' = 0$, are perturbed by the nearby $e\,^3\Sigma^-(v = 1)$ and $d\,^3\Delta(v = 4)$ electronic states. Accurate term values for the first few vibrational levels for the $A\,^1\Pi$ state are available from Field,[12,13] and are the result of an extensive perturbation analysis. These data, along with the ground state term values, which are satisfactorily calculated using the Dunham expansion, have made possible a complete rotational assignment of the LIF spectra.

The population of a single rovibronic state $N(v'',J'')$ is related to the corrected intensity of the transition $I(v'',J'' \leftarrow v'',J'')$ by[14]

$$N(v'',J'') \propto \frac{I(v',J' \leftarrow v'',J'')g(J'')}{S(J',J'')F(v',v'')}, \quad (1)$$

where $S(J',J'')$ is the Hönl–London factor for the $A\,^1\Pi \leftarrow X\,^1\Sigma^+$ transition,[15] $g(J'')$ is the rotational degeneracy $(2J'' + 1)$, and $F(v',v'')$ is the Franck–Condon factor. Rigorously, the intensity of a transition is proportional to the integrated area of the spectral peak. For the purposes of this analysis however, peak heights were determined to be a satisfactory alternative to the peak area.

A thermal rotational distribution (within a single vibrational level) is given by the Boltzmann expression,

$$N(J'') = (2J'' + 1)\exp[-BJ''(J'' + 1)/kT], \quad (2)$$

where B is the ground state rotational constant, k is the Boltzmann constant, and T is the rotational temperature. From Eqs. (1) and (2), a plot of $\ln(I/S)$ vs $J''(J'' + 1)$ will, for a Boltzmann distribution, give a straight line with slope $-B/kT$. While there is no reason to assume *a priori* that the CO rotational distribution will be described by a thermal distribution, plotting the data in this form (a so-called "Boltzmann plot") can provide a measure of the nonthermal behavior of the distribution.

b. Supersonic free jet data. Boltzmann plots for $v'' = 0$, 1, and 2 are presented in Fig. 2. A linear least squares fit to the data is shown for each vibrational level. Experimental points fall relatively close to this line, indicating that the photofragment rotational distributions (for each v'') can be described predominantly by a single temperature. For clarity, only Q-branch data are plotted in Fig. 2; P- and R-branch data are also scattered around the line. Rotational temperatures for each vibrational level are summarized in Table I. The marked difference in the rotational temperature for $v'' = 1$ should be noted, as this is unexpected based on normal statistical arguments which predict decreasing rotational excitation with increasing vibrational excitation. It should also be noted that the quality of the available free jet

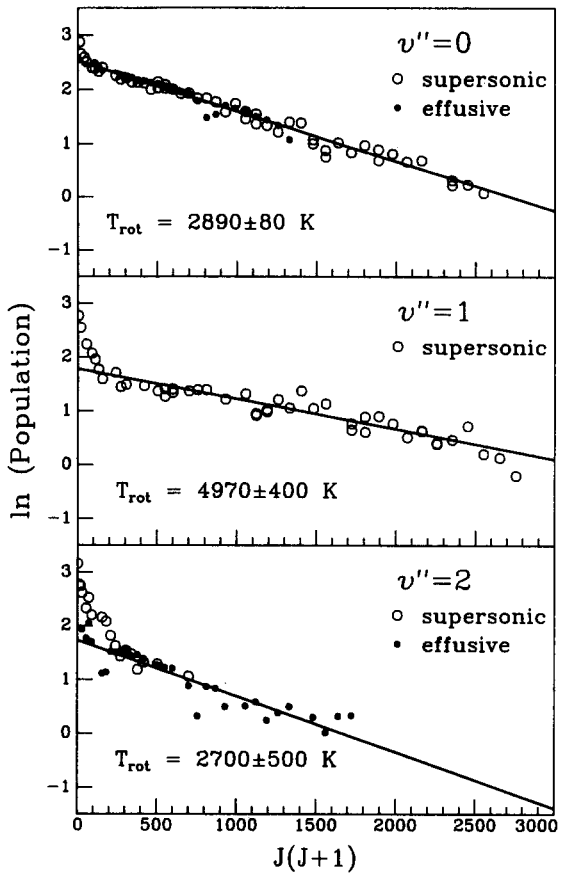

FIG. 2. Boltzmann plots for the CO fragment rotational distribution for $v'' = 0$, 1, and 2 taken in both the supersonic free jet and an effusive beam. The lines shown in the figure are linear least squares fits to the supersonic data for $v'' = 0$ and 1 and to the effusive data for $v'' = 2$.

data for $v'' = 2$ is rather poor in comparison with $v'' = 0$ and 1 and should thus be regarded cautiously.

We have remeasured the $v'' = 0$ spectrum at a delay of 500 ns to explore the effect of collisions on our data. Collisions may serve to rotationally and/or vibrationally relax the CO fragments and thereby skew the observed rotational distribution. The distribution observed under these conditions was fit to a rotational temperature of 2550 ± 300 K, comfortably within the experimental limits of the result obtained from the 200 ns data (2890 ± 80 K, Table I). We therefore conclude that collisions are not creating any noteworthy aberrations in the measured distributions.

c. Effusive beam data. Distortions of observed photofragment energy distributions due to the presence of clusters are always a concern in experiments using supersonic expansions.[16] We have investigated directly whether the presence of clusters in the expansion affects our data by utilizing the cluster-free conditions provided by an effusive beam. A Boltzmann analysis of the $v'' = 0$ distribution, obtained with the effusive source (solid circles in Fig. 2), yielded a rotational temperature of 2920 ± 100 K, virtually identical to the 2890 K temperature obtained from the free jet data. This would seem to indicate that while acetone clusters may be present in the supersonic jet, either their concentration is small, or at least they are not interfering with the measurement of the nascent CO population from the dissociation of acetone monomers.

TABLE I. Nascent rotational and vibrational energy distributions of the CO fragment.

v''	Relative population (%)	T_{rot} (K)[a] Supersonic	T_{rot} (K)[a] Effusive
0	73	2890 ± 80	2920 ± 100
1	20	4970 ± 400	···
2[b]	7	···	2700 ± 500
	$T_{vib} = 2700 \pm 250$ K		

[a] Errors are $\pm \sigma$.
[b] From effusive beam data.

It was found that the effusive beam spectra were a factor of 10 enhanced in the signal-to-noise ratio over the supersonic beam spectra. This stems from a difference between the number of absorbing states in the effusive and supersonic beam experiments. Only small features are observed in the free jet absorption spectrum near 193 nm, with rotational contours 30–40 cm^{-1} broad.[6] At room temperature the rotational widths are approximately 250 cm^{-1} and much hot band structure is observed allowing us to excite more acetone molecules in the effusive beam. The $v'' = 2$ distribution, remeasured in the effusive beam, allowed us to obtain rotational populations to $J'' > 45$ and to attach a much better estimate to the rotational temperature (see Table I). The data from both supersonic and effusive beam measurements are presented in Fig. 2. The data are in tacit agreement for $J'' > 15$, though the free jet data appear to deviate from the effusive beam data in the low J region. Given the relatively poor signal-to-noise of the free jet data, we attach little significance to this deviation. It may be that the small excess population in our low-J supersonic beam data comes from the dissociation of clusters.

2. Vibrational distribution

The relative vibrational population of the nascent CO fragment has been determined by utilizing spectral regions where bands probing two different vibrational states overlap. Specifically, the 1–1, 3–2, and 4–3 bands all have regions of overlap with the 0–0 band. The overlap region was carefully recorded, and relative populations were obtained by dividing the spectral peak intensities by their Franck–Condon factors and rotational terms, as dictated by Eq. (1). The more complete rotational distributions for $v'' = 0$ and 1, obtained from the 2–0 and 0–1 bands, were then scaled to match the data from the 0–0 and 1–1 bands, and are shown in Fig. 3. The P and R branches have been omitted also from this figure for clarity. The solid lines in Fig. 3 provide fits of each data set to a Boltzmann rotational distribution at the temperatures given in Table I.

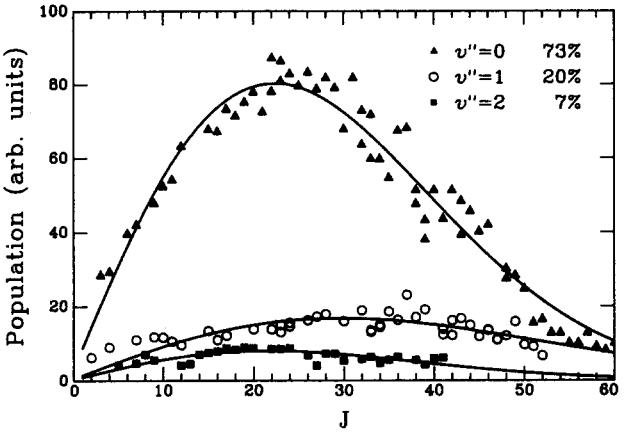

FIG. 3. Rotational distributions of the CO photofragment in $v'' = 0$, 1, and 2 scaled to reflect the relative vibrational populations. Data for $v'' = 0$ and 1 were taken in a supersonic free jet, $v'' = 2$ in an effusive beam.

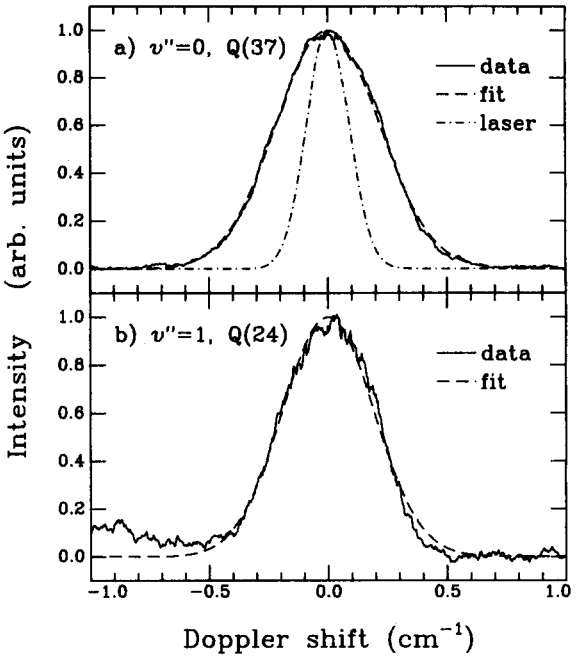

FIG. 4. Doppler profiles of two CO fragment rovibronic transitions: (a) $Q(37)$ of $v'' = 0$ and (b) $Q(24)$ of $v'' = 1$. Each trace is the sum of several experimental measurements. The dashed line is a least squares fit to a Gaussian function. The laser linewidth is indicated on the upper figure.

The total population contained in a vibrational level is simply the sum of population over all the rotational levels. We have summed each of the distributions given by the solid-line Boltzmann curves in Fig. 3 from $J'' = 0$ to J_{max} where J_{max} corresponds to the maximum J'' which may be populated given the available energy.

The data for $v'' = 2$ shown in Fig. 3 are from the effusive source. The $v'' = 0$ to 1 population ratio calculated from the effusive beam data was found to be consistent with the supersonic jet result (again suggesting that clusters in the beam are not affecting the data). We therefore once more take advantage of the superior signal-to-noise of the effusive beam data to obtain a better estimate of the relative population of $v'' = 2$.

The 4–3 bandhead (probing population in $v'' = 3$) is known to lie near the 1–1 bandhead. We were unable to assign this feature consistently and we therefore place an upper limit on $N(v'' = 3) \leqslant 1/2 N(v'' = 2)$. The overall vibrational distribution is summarized in Table I. This distribution is also well fit by a Boltzmann function yielding a vibrational temperature of 2700 ± 250 K.

B. CO fragment translational energy

We have recorded high-resolution Doppler profiles of several CO rovibronic transitions in $v'' = 0$, 1, and 2. Representative spectra, the composite averages of several individual scans, are presented in Fig. 4. The Doppler line shapes appear to be Gaussian, with widths typically on the order of 3 times the laser linewidth (0.6 cm^{-1} vs 0.21 cm^{-1}). A Gaussian line shape is consistent with an isotropic Maxwell–Boltzmann distribution of velocities.[17,18] The relationship between the FWHM of the Doppler profile $\Delta\nu$, the center frequency ν_0, and the temperature characterizing the Boltzmann translational distribution is

$$T_{trans} = (\Delta\nu/2\nu_0)^2 mc^2/2k \ln 2, \qquad (3)$$

where m is the molecular mass and k is the Boltzmann constant.

The profiles in Fig. 4 (and several others) were fit by a Gaussian function using a nonlinear least squares fitting routine. The translational temperature and energy are thus determined from the fits to the data and Eq. (3). Typical linewidths of the profiles are about 0.5–0.6 cm^{-1}, and hence the average translational energy is 3000 ± 400 cm^{-1} (36 ± 5 kJ/mol). There is no apparent difference between the shapes of any of the profiles which might indicate the presence of a vector correlation in the dissociation,[18] although the Q branches appear to be slightly wider than the corresponding P or R branch for similar J. This difference is fairly subtle, and might simply be an experimental artifact stemming from the disparate relative line strengths of the transitions, rather than evidence of a dynamical process.

C. Methyl fragment internal energy

The internal energy distribution of the methyl fragments was measured using $(2 + 1)$ resonantly enhanced multiphoton ionization spectroscopy through the $3p\,^2A_2'' \leftarrow 2p\,^2A_2''$ Rydberg transition of the methyl radical. Methyl ions were mass selected in a TOF-MS, and monitored as the probe laser was scanned across the rovibronic resonances of the Rydberg transition.

The MPI spectrum of the nascent methyl photofragments is presented in Fig. 5. No discrete rotational structure is evident, the resolution limited to vibrational bands. Do-

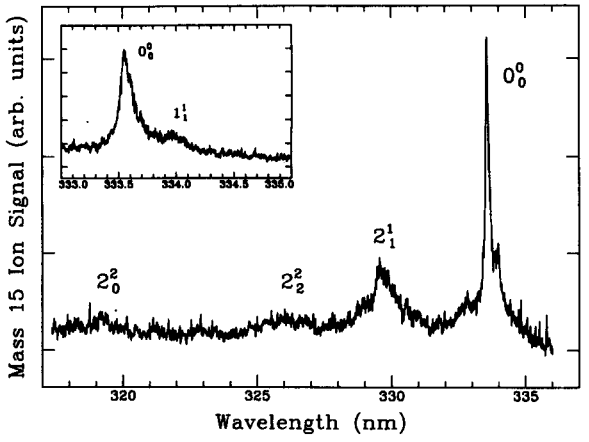

FIG. 5. Multiphoton ionization spectrum of the methyl photofragment from the 193 nm dissociation of acetone. The spectrum is dominated by a large origin band near 333.5 nm and contains the first the few sequence transitions of the ν_2 "umbrella" vibration. Inset is the origin band on an expanded wavelength scale to show the 1_1^1 sequence transition.

minating the spectrum is an extremely large origin band. Also present are the first few sequence bands of the ν_2 out-of-plane bending (umbrella) mode.

Approximately 90 cm^{-1} to the red of the origin is another small band (see inset, Fig. 5). This position is consistent with the assignment 1_1^1.[19,20] Since the excited state frequencies of ν_3 and ν_4 are not known, it is possible that some of the intensity in the origin region might be due to excitation in those vibrations as well. For the purposes of discussion, however, we shall assume that all of this intensity is due to the ν_1 sequence transition.

1. Rotational distribution

The methyl radical is a planar, symmetric top. The $3p\,^2A_2'' \leftarrow 2p\,^2A_2''$ transition is electric dipole forbidden through a single photon, but allowed for two photons. Rotational selection rules for this two-photon transition are: $\Delta K = 0$, with $\Delta N = 0, \pm 2$ for $K = 0$ and $\Delta N = 0, \pm 1, \pm 2$ for $K \neq 0$.[20] Vibronic bands which have similar rotational constants in the initial and final states result in a spectrum which has a strong overlapping Q branch and simple O, P, R, and S branches.

Discrete rotational structure could not be resolved in our spectra. Acquisition of rotationally resolved spectra was inhibited by the readiness with which these bands are power broadened. The laser power could not be reduced sufficiently to give rotationally resolved spectra without incurring an almost complete loss of signal, therefore a compromise had to be reached between signal level and resolution. Nevertheless, an estimate of the rotational excitation imparted to the methyl fragment can be obtained by performing a rotational contour analysis of the origin band. The Q branch is anomalously large, as has been reported previously,[21] and we did not attempt to match its intensity in the simulation. Instead, the simulation of the rotational contour was confined to matching the breadth of the O, P, R, and S branches. An estimate of 500 ± 300 K was obtained for the rotational temperature of the 0_0^0 band.

2. Vibrational distribution

A determination of the vibrational state distribution of the methyl fragment is difficult because predissociation of different MPI intermediate states may occur at different rates, thereby giving rise to inconsistent ionization efficiencies. This complication can be avoided by comparing transitions which access the same intermediate state. The $\Delta v = 0, \pm 2n$ selection rule for nontotally symmetric vibrations, however, further impedes the analysis by preventing a direct comparison between odd and even vibrational levels. Our spectra do not contain bands accessing the same intermediate state, and therefore we cannot carry out a completely rigorous determination of the vibrational state population.

An estimate of the extent to which the predissociation rates differ may be made by comparing the ionization efficiency of bands which sample the same vibrational state population but access a different intermediate state. The populations determined from the integrated area of each of these bands (divided by the Franck–Condon factor[22]) will differ to the extent that the predissociation rates of the intermediate states differ. Specifically, the 1_0^1 and 2_0^2 bands of the CH_3 spectra from Hudgins *et al.*[20] and the 2_1^1 and 2_1^3 bands of methyl obtained from the photolysis of CH_3NO_2 obtained in our laboratory[22–24] were used as test cases. The ionization efficiencies in both cases appear to differ by no more than a factor of 2, indicating that for these pairs of excited state levels, ($1^1, 2^2$ and $2^1, 2^3$), the predissociation rates are not too different. We therefore feel justified in making the approximation that the rates are *similar* for all the intermediate levels that we utilize. This allows us to obtain an estimate of the vibrational distribution for the methyl photofragment.

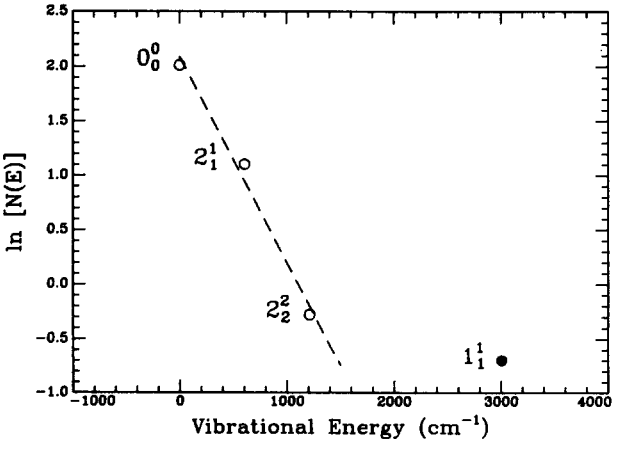

FIG. 6. Boltzmann plot of the methyl fragment vibrational distribution. The open circles are data points for ν_2 (the methyl "umbrella" motion) and the solid circle is for ν_1 (symmetric stretch). The dotted line is a linear fit to the ν_2 data, corresponding to a temperature of 800 ± 300 K.

A Boltzmann plot of the methyl vibrational distribution is presented in Fig. 6. (Note that the value for ν_1 is a maximum, calculated assuming a Franck–Condon factor of 1.0 for the transition.) The data for ν_2 were fit by a line, the slope of which corresponds to a vibrational temperature of 800 ± 300 K. The datum for ν_1 clearly does not fall on the line. Given the paucity of data, no attempt was made to assign a temperature to this degree of freedom.

D. Methyl fragment translational energy

Photofragment recoil velocities can be determined through the application of a pulsed extraction field in the time-of-flight mass spectrometer. The essence of the technique is to allow nascent fragment ions to recoil with the velocity imparted to them by the dissociation for a prescribed period of time before the extraction field is applied. Because the acceleration felt by an ion is a function of its initial position within the electric field at the time when the high voltage is pulsed on, the arrival time is directly related to the projection of the recoil velocity onto the axis of the flight tube. The pulsed field technique and the methods used to transform the arrival time distribution into a velocity distribution are described in more detail in an Appendix (see also Refs. 11, 21, and 23).

The arrival time profile of the methyl fragment was measured over a range of delay times and accelerating voltages. A typical example, obtained with a 500 ns delay and 1000 V accelerating field, is presented in Fig. 7(a). This arrival time profile was converted into a distribution of recoil velocities along the flight tube axis (assuming an isotropic distribution of fragments), using the technique described in the Appendix. The results are presented in Fig. 7(b). Only half the distribution is represented; the other half would contain redundant information and is contaminated by overlapping signal from a lighter fragment ion produced in the mass spectrometer.

The data in Fig. 7(b) were fit by a Gaussian function, represented by the solid line in the figure. Exactly analogous to the Doppler analysis, a Gaussian velocity profile indicates a Maxwell–Boltzmann distribution of speeds. The velocity distribution, converted into a molecular speed distribution, is presented in Fig. 7(c), along with the same transformation applied to a smoothed data set.[25] The average lab frame translational energy of the methyl radical, obtained directly from the fit parameters, is 44 ± 8 kJ/mol, corresponding to an rms velocity of 2400 ± 200 m/s.

To test the validity of the analysis procedure, a reverse transformation was applied to the fit to see how well it replicated the original data. [This is the solid line in Fig. 7(a).] Although some features of the data are not well represented (see the Appendix), the fit does appear to be representative of the average methyl kinetic energy.

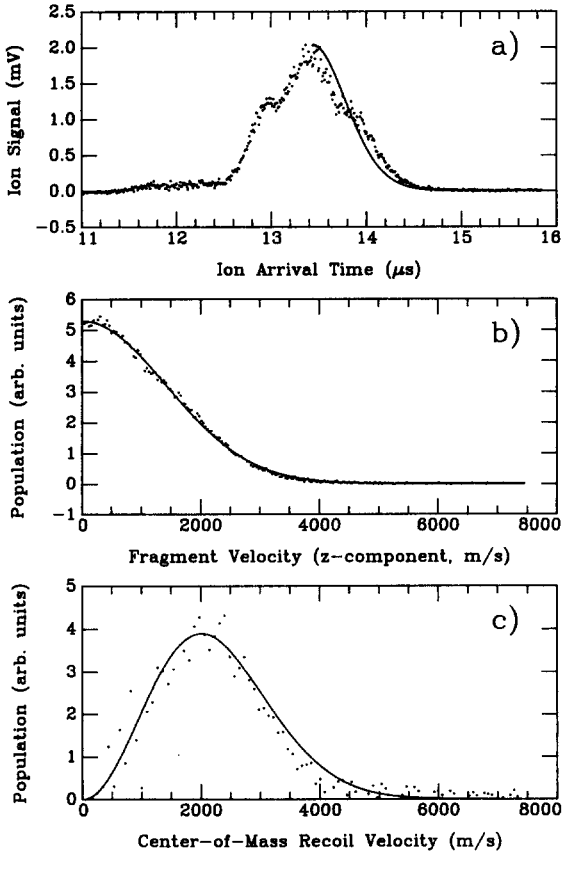

FIG. 7. (a) Pulsed field arrival time distribution for the methyl fragment ionized at the peak of the 0_0^0 band. The fit to the data is a backtransformation from the fit in (b) into arrival time; (b) recoil velocity distribution and a Gaussian fit to the data; (c) the data (smoothed) and fit from (b) transformed into a center-of-mass speed distribution.

E. Average energy of fragments

Although the photofragments are formed with a range of internal and translational energies, it is advantageous for calculation purposes to make use of an average or "typical" energy. The values obtained from our experimental measurements (calculated below) are summarized in Table II.

TABLE II. Average observed fragment energies and model predictions.

		Energy (kJ/mol)		
		Observed	Statistical model	Impulsive model
CH_3	Vib	5	55	11
	Rot	6	···	
	Trans	44	···	44
CO	Vib	10	9	16
	Rot	28	···	27
	Trans	36	···	42
CH_3^+	Vib	5	55	15
	Rot	6	···	
	Trans	44	···	66
		184		221

Rotational energy: The average energy contained in the rotational degrees of freedom can be calculated from the rotational temperature (T_{rot}) using the relations $E_R = (3/2)kT_{rot}$ for nonlinear polyatomic molecules and $E_R = kT_{rot}$ for linear or diatomic molecules. From our estimate of the rotational temperature of the methyl fragments (500 K), we estimate $E_R(CH_3)$ to be 6 kJ/mol. For the CO fragment, E_R is the weighted sum of the average rotational energy in each vibronic level $\Sigma c_n kT_n$, where c_n is the fractional population in v_n'' (from the vibrational distribution) and T_n is the rotational temperature in v_n'' (see Table I). We thus estimate $E_R(CO)$ to be 28 kJ/mol.

Vibrational energy: The energy deposited in vibrations of the fragments can be evaluated as the sum of the energy partitioned into each vibrational level: $E_V = \Sigma c_n(E_n - E_0)$, where c_n is the fractional population in v_n'', and $(E_n - E_0)$ is the quantized vibrational energy in v_n'' with respect to the zero point energy. The calculated values are 10 kJ/mol in CO vibration and 5 kJ/mol in CH_3 vibration.

Translational energy: The average CO translational energy is determined from the CO Doppler profiles to be $(3/2)kT_{trans} = 36$ kJ/mol (corresponding to an rms velocity of 1600 m/s). The methyl translational energy can be determined directly from the Gaussian fit to the TOF arrival time distribution [Fig. 7(b)], for which $(3/2)kT_{trans} = 44$ kJ/mol ($v_{rms} = 2400$ m/s).

IV. DISCUSSION

A. The mechanism of acetone photodissociation

It is well established that excitation of the 3*s* Rydberg state of acetone results in the production of two methyl radicals and carbon monoxide.[3] The reaction mechanism can be written either as a single, concerted process:

$$CH_3COCH_3 \rightarrow CH_3 + CO + CH_3', \quad (4)$$

or as two distinct kinetic steps:

$$CH_3COCH_3 \rightarrow CH_3CO + CH_3, \quad (5a)$$

$$CH_3CO \rightarrow CO + CH_3'. \quad (5b)$$

Before proceeding with the discussion it is necessary to clarify what is meant by some of the terms used. In particular, there would appear to be some ambiguity as to what exactly is meant by the terms "concerted" and "stepwise" and "synchronous." A widely accepted definition of a concerted reaction is "one that takes place in a single kinetic step without necessarily being synchronous,"[26] whereas a synchronous reaction is one in which all the bond breaking steps proceed simultaneously *and* at the same rate. A stepwise reaction, as the name implies, is defined as one which "takes place in two kinetically distinct steps, via a stable intermediate."[26] Experimentally, the difference between a stepwise and a concerted process obviously rests with the detection of the intermediate species. The distinction between a synchronous and nonsynchronous concerted mechanism should be reflected in the distribution of energy in the photofragments. A synchronous process must by definition produce two methyl fragments with identical (rotational, vibrational, and translational) energy distributions. The converse, however, is not necessarily true; a nonsynchronous dissociation could give rise to nearly indistinguishable methyl fragment energy distributions.

The energy level schematic for 193 nm photodissociation of acetone is presented in Fig. 8. The energetics of the fragmentation steps are calculated from the thermochemical heats of formation[27] or from references in the figure.[6,28-30] A 193 nm photon is equivalent to 619 kJ/mol. As illustrated in the figure, the primary fragmentation step [Eq. 5(a)] producing methyl and acetyl is 350 kJ/mol endothermic, and subsequent fragmentation of acetyl [Eq. 5(b)] is endothermic by a further 48 kJ/mol. The overall process [Eq. (4) or (5a) and (5b)] leaves 221 kJ/mol of excess energy to be partitioned among the internal and translational degrees of freedom of the final products, two methyl radicals and a CO molecule.

In the discussion to follow below, the observed energy distributions are used to develop a model for the dissociation dynamics of acetone excited to the 3*s* Rydberg state. First, momentum and energy conservation laws are applied to verify the internal consistency of the observed distributions of translational, rotational, and vibrational energy in the fragments. Next, these distributions are compared to the predictions of simple statistical and impulsive models of the dissociation dynamics, and the results of that comparison are used to construct a description of the dissociation process. Finally, this description is compared with that obtained from previous investigations of acetone photodissociation.

B. Conservation laws

1. Conservation of linear momentum

Conservation of linear momentum provides a set of constraints on the observed fragment velocity distribution. In particular, it should be possible to decide whether two indistinguishable methyl velocity distributions with a mean of the

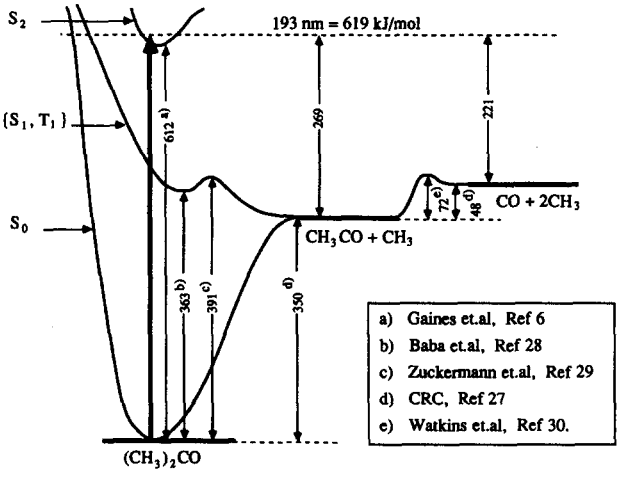

FIG. 8. Energy level schematic for the 193 nm photolysis of acetone. The energy of the 193 nm photon can be seen to lie substantially above each of two small barriers, one on the $\{S_1, T_1\}$ surface leading to the production of acetyl, and one on the surface leading to production of two methyls and CO.

observed value are consistent with the observed CO velocity distribution. For the calculations presented here, the lab frame and the acetone center-of-mass frame are the same, since in all of the experiments the acetone parent has no initial velocity component along the detection axis, i.e., the molecular beam axis is perpendicular to the detection axis.

First, consider a concerted and synchronous process, simultaneously producing all three fragments. A vector diagram representing this process is presented in Fig. 9(a). Since by hypothesis the two bonds break at the same time and at the same rate, the rms velocity of each methyl must be the same and is taken to be the measured average value of 2400 m/s. The CO rms velocity is 1600 m/s, and must bisect the angle between the methyl velocity vectors. Conservation of linear momentum predicts an acetone C–C–C bond angle (on the dissociative surface) of 103°. This angle seems too small (the geometry of acetone in the excited state is not well known, but the angle is probably $\geqslant 120°$), so although this calculation shows that a synchronous process may be consistent with conservation of linear momentum, it is perhaps unlikely.

Next, consider a nonsynchronous process. In this case, since the two bonds break at different instants, there are two reference frames in which linear momentum must be conserved. The velocity of the primary methyl is measured directly in the laboratory frame; its linear momentum is equal and opposite to that of acetyl. The linear momenta of the CO and secondary methyl fragment are equal and opposite in the center-of-mass reference frame of the acetyl, which is moving with the recoil velocity imparted to it by the primary dissociation step. The velocities of the secondary methyl and CO measured in the laboratory reference frame must therefore reflect the recoil velocity of the acetyl.

An isotropic, Maxwell–Boltzmann distribution of fragments produces a Gaussian velocity profile (from either Doppler or pulsed field measurements). If both dissociation steps are isotropic, the resulting profile for a secondary fragment, the convolution of two Gaussians, is also Gaussian with an rms (lab frame) velocity related to the rms (acetyl center-of-mass frame) velocities of the component profiles by[31]

$$[v_{\rm rms}(\mathrm{A})]^2 = [v_{\rm rms}(\mathrm{CH_3CO})]^2 + [v'_{\rm rms}(\mathrm{A})]^2. \quad (6)$$

Here A is a secondary fragment (CO or methyl) and the primed velocity refers to the acetyl center-of-mass frame and the unprimed velocities to the laboratory frame. The average lab frame velocity of a secondary fragment may be represented as the vector sum of the acetyl velocity with a recoil velocity in the acetyl center-of-mass (com) frame which is perpendicular to the acetyl velocity.

A vector diagram of the velocities is presented in Fig. 9(b). We shall assume that the lab frame velocity of the primary methyl is our average value of 2400 m/s, and calculate the velocity of the secondary methyl. Conservation of linear momentum with the primary methyl yields an acetyl recoil velocity of 800 m/s. The CO lab frame velocity (1600 m/s), is the resultant of the acetyl velocity (800 m/s) with the CO velocity in the acetyl com frame, calculated to be 1400 m/s. This in turn implies a value of 2600 m/s for the velocity of the secondary methyl in the acetyl com frame. Finally, the velocity of the secondary methyl in the laboratory frame is calculated to be 2700 m/s (the resultant of 2600 and 800 m/s).

The velocities of the two methyl fragments thus appear to be nearly identical (2700 vs 2400 m/s). We therefore conclude that our measurements of the methyl translational energy distribution includes both methyl fragments and that we are not discriminating against a velocity distribution because of some unanticipated intrinsic limitation in the experiment.

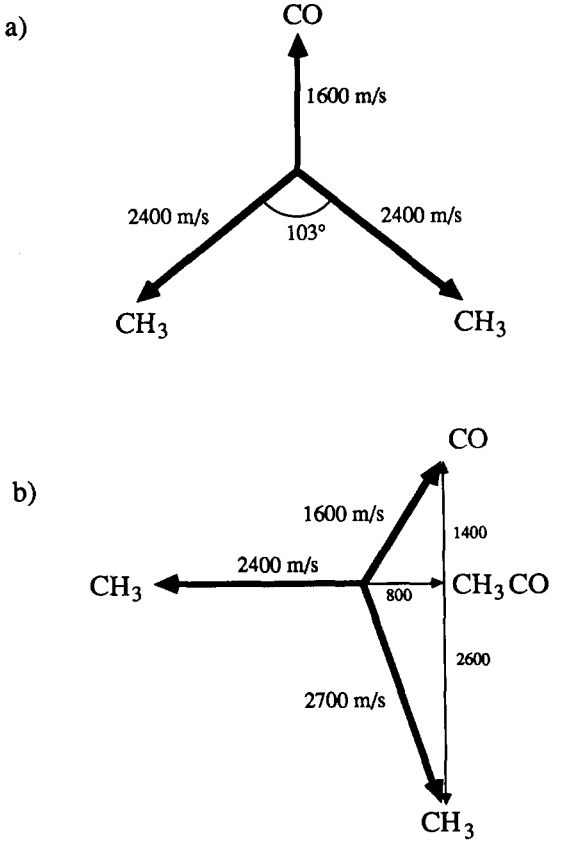

FIG. 9. Newton diagrams demonstrating velocities of the center-of-mass frame (thin lines) and the laboratory frame (thick lines) for (a) synchronous; and (b) nonsynchronous dissociation of acetone.

2. Conservation of energy

Linear momentum conservation, described above, provides a basis for interpreting our methyl translational energy data as the superposition of two almost identical distributions, irrespective of whether the dissociation occurs as a single three-body or as two separate two-body processes. We therefore make the assumption that the experimental methyl measurements are an average over both methyl fragments. The energy released to methyl degrees of freedom is thus simply twice the measured values (Table II) or 110 kJ/mol. Combined with the energy in CO degrees of freedom (74

kJ/mol), the measured total energy released in the 193 nm photodissociation of acetone is 184 kJ/mol, in reasonable agreement with the thermochemical available energy of 221 kJ/mol. Indeed, this discrepancy of ~15% is of the same order as the uncertainty in some of the measurements.

While we are confident in the CO results, it is useful to point out some specific sources of uncertainty in the methyl results. The dominant contribution to the energy released (nearly 50%) is the translational energy of the two methyls. The translational energy distribution was obtained only for ionization at the peak of the Q branch of the 0_0^0 band. The velocity of the fragments probed via this transition may not be representative of the complete population, leading to a bias in the measurements. Experiments to obtain translational energy distributions from other transitions have been unsuccessful due to poor signal to noise on the weaker transitions.

There is also some uncertainty in the relative vibrational populations in the methyl radical, particularly in light of our inability to assign any features to ν_3 or ν_4. One or both of these vibrations might have transitions contributing intensity that has been assigned either to the origin band or to the 1_1^1 band. Another possibility is that vibration/rotation-dependent predissociation in the MPI intermediate state interferes with our ability to detect ν_3 or ν_4. In either case, our calculations would underestimate the vibrational energy in the methyl radical. The relatively small contribution (10%) of methyl vibrations and rotations to the total, however, would require a substantial correction in order to have much overall effect on the interpretation which follows.

3. Conservation of angular momentum

Angular momentum, as well as linear momentum, must be conserved in the dissociation process. Unfortunately, the ambiguity in the value of the orbital angular momentum between the fragments makes it difficult to discuss this aspect of the dynamics quantitatively. Nevertheless, there is vital qualitative information in the distribution of fragment rotations that cannot be ignored.

We first note that CH_3 is produced with relatively modest rotational excitation. This is not surprising, since, in the acetone equilibrium geometry, forces directed along the C–C bonds point directly at the CH_3 center of mass and can therefore generate no substantial angular momentum. The CO fragment, on the other hand, is produced with considerable rotational excitation, significant population extending to $J'' = 60$ and beyond. As has been discussed previously,[8,9] transfer of so much angular momentum is inconsistent with a concerted and synchronous dissociation. In fact, for a planar transition state the resultant of simultaneous forces along the two C–C bonds would be directed along the C–O internuclear axis and could impart no angular momentum to the CO fragment. Even a nonplanar transition state similar to the S_1 equilibrium geometry cannot account for the amount of excitation we measure. Observation of extensive CO rotational excitation is therefore the basis for a strong argument in favor of a nonsynchronous process.

C. Modeling the dissociation dynamics

Classical models of molecular dissociation processes provide a simple framework for analyzing the fundamental features of a complex dissociation event. There are two main classes of such models: statistical and impulsive. Statistical models assume randomization of the available energy throughout the parent molecule prior to dissociation, ignoring interactions between the departing fragments. Impulsive models, on the other hand, partition the available energy on the basis of the classical forces and torques between the interacting species. We apply two of these extreme models to acetone photofragmentation dynamics and discuss the ramifications and shortfalls afterward.

1. Statistical models of energy partitioning

An extremely simple statistical model, applied by Campbell and Schlag to the photodissociation of cyclobutanone,[32] partitions an equal fraction of the available excess energy into each of the vibrational degrees of freedom of the parent molecule. The fraction of the available energy deposited into vibrations of each fragment is then given by the ratio of the number of vibrational degrees of freedom of that fragment to those of the parent molecule.

Applying this model to a synchronous dissociation of acetone yields the following results (see also Table II). There is 221 kJ/mol of available energy, of which 6/24 (55 kJ/mol) is partitioned into the vibrational modes of each methyl, and 1/24 (9 kJ/mol) into CO vibration. While the prediction of the CO vibrational energy agrees well with the experimental measurement of 10 kJ/mol, the vibrational energy carried away by the methyl fragment is grossly overestimated. Only 5 kJ/mol was observed to be in methyl vibration, far less than the 55 kJ/mol predicted by the model. Applying the statistical model to a nonsynchronous dissociation similarly partitions too much energy into methyl vibration. The available energy for the primary dissociation is 269 kJ/mol, of which 6/24 (67 kJ/mol) is partitioned into the primary methyl fragment.

It is perhaps not surprising that so simple a model does not adequately describe the dynamics of a complex dissociation. Therefore a more sophisticated statistical calculation has also been performed. Here a representative (v'',J'') state of CO was chosen, and a statistical prior distribution of energy into the remaining degrees of freedom (methyl vibration and rotation, and translation of all three fragments) was tabulated as a function of total translational energy. For dissociation into three fragments, the density of translational states for the system is proportional to the square of the translational energy.[33,34] For ease of calculation, only the J levels of the CH_3 radicals were counted, each with a statistical weight of $(2J+1)^2$. The components of the degenerate methyl vibrations (ν_3 and ν_4) were counted separately.

The results of two such calculations, for $(v'',J'') = (0,0)$ and $(0,40)$, provided translational energy distributions for comparison with the data. The calculated distribution in each case peaks at an overall translational energy of ~50 kJ/mol, less than 25% of the total available.

[The mean of the distribution is 59 kJ/mol for (0,0) and 52 kJ/mol for (0,40).] Averaging explicitly over all of the available CO states would shift the average to even lower translational energy. By contrast, our observations require an average of ~ 120 kJ/mol in translation. We therefore conclude that any model partitioning energy statistically into the fragment degrees of freedom is inappropriate for describing the dissociation dynamics of this system.

2. Impulsive model of energy partitioning

Impulsive models of molecular photodissociation are based on the assumption that the molecule breaks apart due to vibrational motion, without general equilibration of internal energy. These models use the forces and torques which are produced between the fragments to describe the translational, vibrational and rotational excitation in the separating fragments.

The impulsive model presented by Busch and Wilson[35] treats the dissociation of a triatomic molecule $\alpha\beta\gamma$ using classical formulations of the impulsive transfer of momentum. The basic premise of this model is that the atoms of the dissociating bond α–β recoil sharply and release the energy before the other atom has had time to respond. Initially, γ is considered to be a spectator, and the energy available from the dissociation $E_{\rm avl}$ is partitioned between the recoiling atoms α and β according to conservation of linear momentum. The recoiling atom β then undergoes an inelastic collision with γ. The initial linear momentum of β must be conserved, and it manifests itself as rotation, vibration and translation of the $\beta\gamma$ fragment. According to this model, the total energy partitioned into translation is given by

$$E_T = (\mu_a/\mu_f)E_{\rm avl}, \tag{7}$$

where μ_a is the reduced mass of the two atoms α and β at the ends of the dissociating bond, and μ_f is the reduced mass of the fragments α and $\beta\gamma$. By conservation of momentum, the energy partitioned into vibrational and rotation of $\beta\gamma$ is related to the α–β–γ bond angle χ by

$$E_V = (1-\mu_a/\mu_f)E_{\rm avl}\cos^2\chi, \tag{8}$$

$$E_R = (1-\mu_a/\mu_f)E_{\rm avl}\sin^2\chi. \tag{9}$$

We have generalized this model to apply to polyatomic molecules. Consider the dissociation of polyatomic molecule AB into fragments A and B, each of which may also be polyatomic. Let AB be bonded through atoms α (in A) and β (in B). By analogy to the triatomic system, we define the following quantities: μ, the reduced mass of α and β; $m_{\rm A}$, the mass of A; $m_{\rm B}$, the mass of B; m_α, the mass of atom α; m_β, the mass of atom β. The initial impulse is along the α–β bond, and partitions the available energy $E_{\rm avl}$, between A and B according to the masses of the recoiling atoms α and β:

$$E(\mathrm{A}) = (\mu/m_\alpha)E_{\rm avl}, \tag{10a}$$

$$E(\mathrm{B}) = (\mu/m_\beta)E_{\rm avl}. \tag{10b}$$

The energy is further partitioned into translational and internal (vibrational and rotational) energy of A and B as follows:

$$E_T(\mathrm{A}) = (m_\alpha/m_{\rm A})E(\mathrm{A}), \tag{11a}$$

$$E_T(\mathrm{B}) = (m_\beta/m_{\rm B})E(\mathrm{B}), \tag{11b}$$

$$E_{V+R}(\mathrm{A}) = [1-(m_\alpha/m_{\rm A})]E(\mathrm{A}), \tag{12a}$$

$$E_{V+R}(\mathrm{B}) = [1-(m_\beta/m_{\rm B})]E(\mathrm{B}). \tag{12b}$$

The separation of the internal energy into vibrational and rotational components is a function of the fragment's geometry. Considering the specific case where B is a diatomic β–γ, the distribution has the same dependence on the α–β–γ bond angle χ as presented above for a triatomic molecule [Eqs. (8) and (9)]:

$$E_V(\mathrm{B}) = [1-(m_\beta/m_{\rm B})]E(\mathrm{B})\cos^2\chi, \tag{13a}$$

$$E_R(\mathrm{B}) = [1-(m_\beta/m_{\rm B})]E(\mathrm{B})\sin^2\chi. \tag{13b}$$

Another specific case worth consideration is when the impulse is directed towards the center of mass of fragment A (such as is true for methyl). Strictly speaking, an impulse at the center of mass cannot induce rotation in the fragment, only vibration. Vibrational motion within the parent AB, however, including zero-point motion, can result in a less strict partitioning of the energy. Lacking a simple expression for this partitioning, we consider only the sum of the vibrational and rotational energies of the methyl fragment [Eq. 12(a)].

Application of this model to acetone is still nontrivial. By definition, impulsive models channel *all* of the available energy into the dissociation coordinate. Acetone has two identical channels competing for this energy. The microscopic details of the energy balance will surely depend on the different positions and momenta of the atoms during the dissociation, but the macroscopic *average* energy contained in each dissociation coordinate must be equal, since the two coordinates are identical. The available energy after breaking both C–C bonds is 221 kJ/mol; the average $E_{\rm avl}$ for each impulsive dissociation is thus 110 kJ/mol. Since it is clear from our observation of extensive rotational excitation in the CO that the two C–C bonds cannot break at the same instant, we consider nonsimultaneous impulses in the two coordinates.

The first impulse serves to cleave acetone into the primary methyl and an (already dissociating) acetyl fragment. Application of Eqs. (10)–(13) yields the following results (summarized in Table II). The primary methyl receives 44 kJ/mol as translational and 11 kJ/mol as internal energy, while the recoiling acetyl intermediate receives 16 kJ/mol in translational and 40 kJ/mol in internal energy. The impulse on the acetyl intermediate is very near the center of mass, so the 40 kJ/mol internal energy of the acetyl will be manifested primarily in vibrations.

The recoiling acetyl fragment, already dissociating under the influence of a repulsive potential, receives a 40 kJ/mol kick from the departing methyl, which adds to its internal energy. The coupling between this kick and the dissociative coordinate is unclear. The spirit of impulsive models suggests that it will eventually end up in the dissociative

coordinate. Using this philosophy, the impulsive model results in Table II are calculated. [An acetyl CCO bond angle[36] of 128° was used in Eq. (13), and the acetyl velocity was added to CO and CH_3 velocities according to conservation of momentum.] In fact, it matters little to the qualitative results in Table II whether all or none of the 40 kJ/mol is coupled to the second dissociation. If none contributes to the impulse, then this energy must all end up in vibrations/rotations of the CH_3 and CO fragments, resulting in a 20 kJ/mol decrease in total translational energy and the concommitant increase in internal energy. The actual situation probably lies somewhere between these two extremes.

The predictions of the impulsive model compare very favorably to the experimental results (see Table II). The largest discrepancy is found in the translational energy of the secondary methyl fragment, which the model appears to overestimate. The predictions of the model are constrained to sum to 221 kJ/mol, the available energy. As discussed earlier (Sec. IV B), our observed results sum to slightly less; the difference will be reflected by overestimation by the model.

It needs to be pointed out that although two impulses are treated in a sequential fashion we are not implying two kinetically different steps. In fact the reverse is true. The available energy used in this model (221 kJ/mol) is for the breaking of two C–C bonds in a concerted though nonsynchronous process. Both impulses are proceeding at the same time but with independent phase and force. If we were to treat the acetone dissociation as two kinetically different steps then, in the spirit of the impulsive model, the full 269 kJ/mol should be available to the primary cleavage (see Fig. 8) resulting in a primary methyl translational energy of 107 kJ/mol, 2.5 times the observed value.

D. Dynamical considerations

The impulsive and statistical models represent two extreme descriptions of dissociation dynamics: from complete localization to complete randomization of the available energy. Between lies a continuum of dissociation processes reflecting the extent of energy redistribution, bounded at one end by the impulsive description, and at the other by the statistical description. The axis of the continuum can also be considered to reflect the time scale for dissociation. An impulsive dissociation occurs rapidly, allowing no redistribution; a statistical dissociation is slower, allowing time for the energy to randomize in the molecule.

The dissociation of acetone following excitation to the 3*s* Rydberg state apparently falls near the impulsive end of this continuum. The experimentally observed average energies of the fragments are fit very well by an impulsive model (see above). A specific manifestation of the impulsive nature of the dissociation is the lack of excitation in the methyl internal degrees relative to its translation. The energy in the parent molecule is localized in the dissociating bonds, and the dissociation occurs very rapidly, with little time for redistribution of the energy.

1. Dissociation rates and surfaces

An impulsive dissociation generally suggests excitation onto a directly repulsive (diatomic) surface. The fact that the laser excites a *pre*dissociative Ryderg state of acetone is apparently at odds with an impulsive mechanism. To explain why the dissociation occurs impulsively, we need to examine the electronic surfaces on which the dissociation takes place.

Initial absorption of a 193 nm photon excites acetone to the 3*s* Rydberg state (S_2). In this state, acetone has little excess energy for vibration ($\sim 500\ cm^{-1}$), so little vibrational redistribution is expected to occur. According to Vaida and co-workers,[7] S_2 is predissociative; crossing to the mixed $\{S_1,T_1\}$ surface is effected via motions of the C(CO)C skeleton. The acetone finds itself on this $\{S_1,T_1\}$ surface with $\sim 21\,000\ cm^{-1}$ (250 kJ/mol) of excess energy manifested in skeletal motions. Before vibrational redistribution can transfer this energy into methyl vibrations, both C–C bonds extend with no necessary phase, rate or energy relationship. All barriers to the C–C extension lie well beneath the available energy (see Fig. 8) and should play little part in the dissociation dynamics.

We now evaluate an approximate time scale for the dissociation and a lifetime for the acetyl. RRKM theory is not appropriate here because its basic premise is an equilibrium of vibrational energy which is eventually channeled into the reaction coordinate. The opposite situation is proposed here. Energy is initially placed in the dissociation coordinate and dissociation competes effectively with equilibrium. In molecules the size of acetone a benchmark for complete relaxation is ~ 1 ps.[37] Consequently, the lifetime of $\{S_1,T_1\}$ acetone and/or acetyl must be less than this benchmark, since otherwise the methyl fragments would reflect the redistribution of energy as an increase in internal excitation at the expense of translational energy.

2. Anisotropy and vector correlations of the photoproducts

The translational energy distributions of both the CO and CH_3 fragments observed in this work were modeled as *isotropic* Maxwell–Boltzmann distributions. The isotropy of the distributions received no comment in the Results, but certainly merits some discussion in light of the model proposed for the dissociation.

There is some ambiguity in previous investigations as to whether dissociation of acetone produces an isotropic or anisotropic distribution of fragments. Hancock and Wilson[2] dissociated acetone at 266 nm and observed an isotropic distribution of acetyl and methyl fragments (no CO was observed). Solomon *et al.*[38] on the other hand, observed a highly anisotropic CH_3 distribution following Hg arc excitation (254 nm). Our data (see Figs. 4 and 7) tend a favor an *isotropic* photofragment distribution following 193 nm excitation. It should be added here that the data in Figs. 4 and 7 were obtained using an unpolarized 193 nm laser where the effect of an anisotropy would be somewhat reduced (though not eliminated) over experiments using a polarized photolysis laser.

At first glance an isotropic distribution may appear at odds with the impulsive, three-body dissociation model of acetone presented here. Recall, however, that the initial 193 nm excitation is to the low lying levels of the 3*s* Rydberg surface (S_2). The structured features observed in the S_2–S_0 absorption band[6] indicate that the S_2 surface is bound, dissociation occurring after internal conversion to the strongly coupled $\{S_1,T_1\}$ surface (see Fig. 8). The predissociation rate is unknown; molecular rotation before crossing to the $\{S_1,T_1\}$ repulsive surface will greatly diminish any anisotropy in the spatial distribution of products.

Vaida and co-workers also postulate that one of the modes in coupling the $\{S_1,T_1\}$ and S_2 surfaces is ν_{16}, an out-of-plane skeletal bending mode. This is not surprising since the ground and Rydberg states both have a planar skeleton, whereas the $S_1(n,\pi^*)$ state is pyramidally distorted.[28] Internal conversion from S_2 to $\{S_1,T_1\}$ then likely induces momentum of the departing CO and CH_3 fragments that is perpendicular to the molecular plane, which would also have the effect of reducing the anisotropy of the reaction.

Correlation between the velocity and rotation vectors of the recoiling species would be observed in our Doppler profiles as differences in width or shape between the (*P*,*R*) branches and the *Q* branch of CO. (For extreme examples see Refs. 10 and 21). No consistent difference was observed (although a subtle trend favoring wider *Q* lines was observed under favorable conditions). Profiles of *P*, *Q*, and *R* transitions all appear Gaussian with widths agreeing to within 15% (our experimental uncertainty) in all instances. Vector correlations cannot be eliminated by parent molecular rotation[10] but can certainly be destroyed if the dissociation mechanism is nonplanar. Lack of strong vector correlations therefore leads us to believe that the dissociation of acetone is nonplanar on the $\{S_1,T_1\}$ surface after internal conversion from a longer-lived Rydberg surface which may allow the molecule time to undergo some rotation prior to dissociation.

3. CO fragment rotational distribution

One surprising feature of the CO rotational distributions is that the rotational temperature *increases* from $v''=0$ to 1, and then decreases again for $v''=2$. Simple energetic arguments predict that rotational excitation should *decrease* with increasing vibrational excitation.

A suggestion to explain the anomalously large rotational temperature in $v''=1$ comes from the work in this laboratory on the collisional excitation of CO by hyperthermal (1.6 eV[39] and 2.3 eV[40]) H atoms. In that work, it was observed that collisions which produced a vibrationally excited CO also produced a more highly excited rotational distribution. Classical trajectory calculations indicated that vibrationally inelastic collisions occurred only in a small region of the potential surface localized around the H–C–O minimum (corresponding to a bond angle of 126°). Thus, the small range of impact parameters which result in vibrational excitation favor the production of an excited rotational distribution. The acetyl (H_3C--CO) potential surface may be similar, at least in gross detail, to that of H--CO (both single bonds and similar bond angles—126° for HCO and 128° for acetyl[36]). Thus we might expect a propensity towards coincident (high *v*, high *J*) excitation. There is a limit to the extent to which this trend may be observed however, due to the finite amount of energy available for internal excitation of the fragments. This perhaps accounts for the uniqueness of the $v''=1$ result.

4. Methyl fragment vibrational distribution

The vibrational excitation of the methyl fragment is manifested primarily in the ν_2 "umbrella" mode. A methyl functionality is pyramidal, while a free methyl radical is planar. Physically, one might therefore expect the change from pyramidal to planar geometry to be responsible for excitation of the umbrella mode. Propensity towards excitation of ν_2 is not unique to this study. Almost identical energy disposal into the methyl fragment has been observed in this laboratory for the 193 nm dissociation of nitromethane,[23,24] and the 266 nm dissociation of CH_3I.[22] Other examples may be found in the studies of Hudgins *et al.* on methyl radicals produced from the pyrolysis of dimethyl sulfoxide and ditertiarybutyl peroxide.[20] We have modeled both bond breaking events as impulsive. The force of the impulse is along the center of symmetry of the methyl group, which may excite the ν_2 out-of-plane vibration. The in-plane stretches and bends (ν_1, ν_3, and ν_4) cannot be excited by such an impulse. The ν_2 vibration may also be favored simply on energetic grounds, having the lowest vibrational frequency.

E. Comparison to other studies

The vibrational and rotational temperatures for the CO fragment obtained by Woodbridge *et al.*[9] ($T_{vib} = 2030^{+730}_{-430}$ K; $T_{rot} = 3360^{+1540}_{-800}$ K) in their time-resolved FTIR emission experiments agree very well with our results ($T_{vib} = 2700 \pm 250$ K; $T_{rot} = 2700$–4970 K, depending on the vibrational level). They described the dissociation as nonconcerted, but use this term to mean not synchronous in the nomenclature used here. It was their assumption that the dissociation of acetone was a two-step process, with a stable acetyl intermediate, but they qualified that assumption by stating that the acetyl must dissociate before the internal energy in the skeletal motion of the acetyl can redistribute into methyl motion. With the additional information at our disposal (especially translational energies) we believe that their qualifying statement (placing a short time limit on the acetyl survival) is certainly correct but that the initial assumption is not needed and the rupture of both C–C bonds is occurring nearly simultaneously.

The earlier work of Donaldson and Leone,[8] monitoring infrared emission from the ν_3 methyl vibration, however, is somewhat of a puzzle. They observed emission corresponding to much higher internal excitation ($E_{rot+vib} = 36$ kJ/mol) than we observe (11 kJ/mol). Their observations were of population in excited levels of the antisymmetric C–H stretch ν_3 whereas our observations of

methyl showed significant population only in ν_2, the out-of-plane bend, and to a lesser extent ν_1, the symmetric stretch. The disparity between the results might lie in the detection techniques. The ν_1 and ν_2 modes cannot be observed by the infrared technique, whereas, because of unknown predissociation rates in the methyl intermediate state, the MPI detection efficiency for the ν_3 mode is unknown. Another possible source of the discrepancy can be predicted from our knowledge of the methyl fragment translational energy. Our measured CH_3 velocity distribution is characterized by an rms velocity at least three times greater than would be expected at room temperature, resulting in a collision frequency that is increased by the same factor. These relatively energetic collisions could serve to convert translational energy into vibrational and rotational energy within the 1 μs system response of the infrared emission experiment. In any case, neglect of possible ν_3 population does not substantially affect the conclusions from our model calculations. A statistical model still does not predict as much methyl translational energy as observed, and while the impulsive model would be in less good agreement if there were more methyl vibrational energy than observed in our experiments, the model would still predict correctly the methyl translational energy and the CO internal and translational distributions.

Baba *et al.*[5] have studied the fragmentation of acetone via multiphoton ionization mass spectrometry. They surmised the existence of a stable acetyl intermediate based on a $n = 1.4$ power dependence of the $m/e = 43$ ion signal. An acetyl ion may arise in their experiment from three pathways: (i) fragmentation of the parent acetone ion, (ii) 193 nm dissociation of the acetone ion, and (iii) dissociation of the intermediate acetone state and subsequent direct two-photon ionization of the acetyl fragment. In their experiment it is difficult to determine the predominant pathway for the production $(\text{acetyl})^+$, however, it is not inconceivable that pathway (iii) contributes even for an exceptionally short-lived (or not-yet-free) acetyl. The resonance enhanced two-photon ionization cross section for acetyl is expected to be very large at 193 nm[5] and may compete with the ongoing dissociation process. Although our results cannot rule out the presence of a stable acetyl intermediate, they do suggest that its lifetime is sufficiently short (i.e., less than the vibrational redistribution time) that it would be difficult to observe and identify spectroscopically. A pump–probe experiment with subpicosecond resolution may further elucidate these questions.

V. CONCLUSIONS

Our study of the photodissociation dynamics of acetone following excitation at 193 nm has led to the following conclusions:

(i) Methyl is produced with little internal excitation ($T_{\text{vib,rot}} < 1000$ K), but large translational energy corresponding to an rms velocity of 2400 m/s.

(ii) CO is produced primarily in $v'' = 0$, with a distribution described by a vibrational temperature of $T_{\text{vib}} = 2700$ K, with considerable rotational excitation in all vibrational levels ($T_{\text{rot}} \approx 3000$–$5000$ K), and translational energy corresponding to an rms velocity of 1600 m/s.

(iii) Energy and momentum conservation arguments suggest that the two methyl fragments have nearly indistinguishable energy distributions, each close to our observed average values.

(iv) Angular momentum constraints suggest that the dissociation is nonsynchronous, with an unspecified delay between the two bond cleavage steps.

(v) The dissociation dynamics are described very well by an impulsive model with E_{avl} on average divided equally into the two dissociation coordinates.

(vi) Statistical models of the dissociation, in contrast, partition too much energy into the vibrational modes of the methyl fragment.

These conclusions lead us to describe acetone dissociation at 193 nm in the following manner:

$$(CH_3)_2CO + 193 \text{ nm} \rightarrow (CH_3)_2CO(S_2),$$

$$(CH_3)_2CO(S_2) \rightarrow (CH_3)_2CO\ (\{S_1,T_1\}) \quad k_{\text{ic,isc}},$$

$$(CH_3)_2CO(\{S_1,T_1\}) \rightarrow CH_3 + CO + CH_3 \quad k_{\text{diss}} > k_{\text{vr}}.$$

Note that k_{diss} (the dissociation rate) is faster than k_{vr} (the vibrational redistribution rate) but that $k_{\text{ic,isc}}$ (the internal conversion or intersystem crossing rate) may be much slower so as to allow acetone (S_2) rotation to diminish any fragment anisotropy. Also, the dissociation step is described by a single rate constant. Calculations using two distinct kinetic steps cannot reproduce the data.

ACKNOWLEDGMENTS

This work was supported by the Department of Energy under Grant No. DE-FG02-88ER13934 and by the National Science Foundation under Grant No. CHE-86-17062. KAT gratefully acknowledges the Proctor & Gamble Company and the Dow Chemical Company for graduate fellowships. This work was done in cooperation with the research program of Yehuda Haas under a US–Israel Binational Science Foundation Grant. We also acknowledge Dr. Gunjit Chawla for assistance in the initial attempts at obtaining the VUV-LIF spectra, and Rachel Ogorzalek Loo for initial advice on the pulsed field switching technique. Professor Itamar Burak and Professor A. Ben-Reuven provided useful discussions about prior distributions.

APPENDIX: ANALYSIS OF PULSED FIELD TIME-OF-FLIGHT SPECTRA

The principle underlying the pulsed field technique is the same as that for Doppler spectroscopy, namely to exploit an inherent anisotropy in the detection apparatus to measure the distribution of velocities of a molecular species with respect to the unique axis. In the case of the pulsed field technique, the unique axis is determined by the accelerating field(s) of the mass spectrometer.

The kinetic energy imparted to an ion is a function of its position within the accelerating field. The arrival time, in turn, will be a function both of that position and the initial velocity, if any, of the ion at the instant it first feels the influence of the field. In the pulsed field technique, photofragments are generated by the photolysis laser and ionized by the probe laser in the absence of any external fields. The fragment ions thus recoil from an effective point source with the velocities imparted to them by the dissociation.

At the moment the extraction pulse is turned on, both the position and the velocity of a fragment ion are determined only by the initial recoil velocity. We are concerned specifically with the projection of the velocity onto the flight tube axis, designated z. The center of the observed ion arrival time distribution will be comprised of those ions with essentially no recoil velocity component along z. The greater the ion's velocity component along z, the further it will be shifted in time from the center of the distribution, so the edges of the distribution correspond to those ions with the greatest recoil velocities.

The arrival time of an ion $t_{\rm arr}$ is therefore a function of the component of its recoil velocity along the z axis v_z as well as the charge/mass ratio q/m, the electric field E, and the delay time before the high voltage is applied to the repeller plate t_d. The expression of $t_{\rm arr}$ in terms of v_z is fairly straightforward to derive using the equations of classical mechanics to describe the behavior of a charged particle in accelerating and field-free environments:

$$t_{\rm arr} = t_d + z_f/v' + (v' - v_z)/a_z, \qquad \text{(A1)}$$

where $v' = [v_z^2 - 2a_z(v_z t_d - z_a)]^{1/2}$ and $a_z = qE/m$. z_f is the length of the field-free drift region, z_a is the length of the acceleration region traveled by an ion with zero recoil, a_z is the acceleration imparted to the ion by the electric field E,[41] and v' is the instantaneous velocity of the ion upon entering the drift region.

In general, we wish to transform from $t_{\rm arr}$, the experimentally determined quantity, to v_z. Inverting the expression for $t_{\rm arr}$ results in the following third-order polynomial in v_z:

$$\begin{aligned} 0 = {} & v_z^3[2t_{\rm arr}] \\ & + v_z^2[a_z t_{\rm arr}^2 - 6a_z t_{\rm arr} t_d + a_z t_d^2 - 2(z_f + z_a)] \\ & + v_z[a_z\{4z_a t_{\rm arr} + 4(z_a + z_f)t_d - 2t_d a_z (t_{\rm arr} - t_d)^2\}] \\ & + a_z\{2z_a a_z (t_{\rm arr} - t_d)^2 - (z_f^2 + 4z_a z_f + 4z_a^2)\}. \end{aligned} \qquad \text{(A2)}$$

Using this equation with the values of z_a and z_f appropriate for our time-of-flight mass spectrometer (1.27 and 106 cm, respectively) it is possible to correlate the observed arrival time of a fragment with the z component of its recoil velocity.

The distribution of v_z corresponds to the projection of the sphere of recoiling ions onto the z axis. For an isotropic distribution of fragments recoiling with a single speed (i.e., the speed distribution is a delta function), the spatial distribution of fragments is a sphere of infinitesimal thickness and the projection of this distribution onto the z axis is a rectangle [see Fig. 10(a)]. A distribution of speeds then corresponds to a z component velocity distribution which is the sum of many such rectangles, each with a width equal to the velocity and an area proportional to the number of fragments with that velocity [Fig. 10(b)]. The intensity at each point along the distribution can therefore provide information about the number of ions that are recoiling with the corresponding speed.

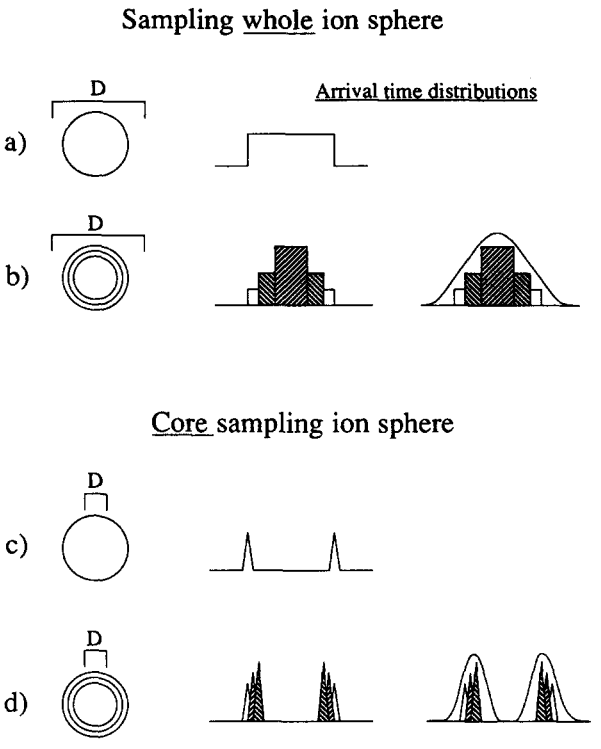

FIG. 10. Hypothetical pulsed field time-of-flight experiments assuming an isotropic spatial distribution of fragments. Arrival time distributions are shown after detecting either the whole ion sphere or by core sampling the ion sphere ("D" is the detector): (a) single fragment velocity detecting complete ion sphere; (b) multiple fragment velocities detecting complete ion sphere; (c) single fragment velocity obtained under core-sampling conditions; (d) multiple fragment velocities obtained under core-sampling conditions.

Under certain conditions, the ion sphere is larger than the detector, and only the "core" is collected; that is, only those ions with a relatively small velocity component perpendicular to z impact on the detector. In the case of the isotropic distribution of ions traveling at a single speed, the distribution is expected to have intensity only at the wings [Fig. 10(c)], since those ions which previously arrived in the center are not detected.

The summation of these profiles over a spread of velocities [Fig. 10(d)] is not trivial; the fraction of ions with a given velocity collected at the detector is a function of that velocity. To extract correctly the intensity information from such a distribution, care must be taken to account properly for the detection sensitivity at each velocity. In addition, it is first necessary to transform the distribution from arrival time to velocity in order to remove the asymmetry introduced by the continuing expansion of the ion sphere as it crosses the plane of the detector.

The analysis is carried out in the following manner. Working from one edge of the distribution to the center, the abscissa of the raw data is converted from arrival time to v_z. Simultaneously, the ordinate is compared to the previous point. The difference (effectively the derivative at that point) is attributed to the current velocity. The fraction (if any) of ions lost due to core sampling is also calculated and added to the remainder of the data set. The resulting z component velocity distribution is either fit to an *a priori* functional form (e.g., a Gaussian) or to a smoothed spline, and then transformed to a lab frame recoil velocity distribution.

The process is illustrated in Fig. 7 of the main text. It is interesting to note that features that would appear to be of interest in the raw data are obscured by the correction for "core sampling." While the resulting velocity distribution [Fig. 7(b)] is well fit by a Gaussian, the reverse transformation of that Gaussian [Fig. 7(a)] does not reproduce the shoulder that appears in the data. This illustrates the unusual sensitivity of the pulsed field technique to fluctuations in the velocity distribution, particularly for small recoil velocities. It also points up the need for caution in analyzing data of this type to be certain that the results are not being distorted by artifacts of the detection conditions.

[1]E. K. C. Lee and R. S. Lewis, Adv. Photochem. **12**, 1 (1980).
[2]G. Hancock and K. R. Wilson, in *Proceedings, 4th International Symposium on Molecular Beams* (Peymeinada, Cannes, France, 1973).
[3]M. Brouard, M. T. MacPherson, M. J. Pilling, J. M. Tulloch, and A. P. Williamson, Chem. Phys. Lett. **113**, 413 (1985).
[4]P. D. Lightfoot, S. P. Kirwan, and M. J. Pilling, J. Phys. Chem. **92**, 4938 (1988).
[5]M. Baba, H. Shinohara, N. Nishi, and N. Hirota, Chem. Phys. **83**, 221 (1984).
[6]G. A. Gaines, D. J. Donaldson, S. J. Strickler, and V. Vaida, J. Phys. Chem. **92**, 2762 (1988).
[7]D. J. Donaldson, G. A. Gaines, and V. Vaida, J. Phys. Chem. **92**, 2766 (1988).
[8]D. J. Donaldson and S. R. Leone, J. Chem. Phys. **85**, 817 (1986).
[9]E. L. Woodbridge, T. R. Fletcher, and S. R. Leone, J. Phys. Chem. **92**, 5387 (1988).
[10]I. Burak, J. W. Hepburn, N. Sivakumar, G. E. Hall, G. Chawla, and P. L. Houston, J. Chem. Phys. **86**, 1258 (1987).
[11]R. Ogorzalek Loo, G. E. Hall, H.-P. Haerri, and P. L. Houston, J. Phys. Chem. **92**, 5 (1988).
[12]R. W. Field (unpublished results).
[13]A. C. Le Floch, F. Launay, J. Rostas, R. W. Field, C. M. Brown, and K. Yoshino, J. Mol. Spectrosc. **121**, 337 (1987).
[14]G. Herzberg, *Spectra of Diatomic Molecules*, 2nd ed. (Van Nostrand Reinhold, New York, 1950), pp. 127,201.
[15]Hönl–London factors for the case $\Delta\Lambda = +1$ are: $S^R = J'' + 2$, $S^Q = 2J'' + 1$, and $S^P = J'' - 1$. G. Herzberg, *Spectra of Diatomic Molecules*, 2nd ed. (Van Nostrand Reinhold, New York, 1950), pp. 127,208.
[16]See, for example, N. Sivakumar, I. Burak, W.-Y. Cheung, P. L. Houston, and J. W. Hepburn, J. Phys. Chem. **89**, 3609 (1985).
[17]A. C. G. Mitchell and M. W. Zemansky, *Resonance Radiation and Excited Atoms* (MacMillan, New York, 1934), p. 99.
[18]P. L. Houston, J. Phys. Chem. **91**, 5388 (1987).
[19]P. L. Holt, K. E. McCurdy, R. B. Weisman, J. S. Adams, and P. S. Engel, J. Chem. Phys. **81**, 3349 (1984).
[20]J. W. Hudgins, T. G. DiGuiseppe, and M. C. Lin, J. Chem. Phys. **79**, 571 (1983).
[21]R. Ogorzalek Loo, C. E. Strauss, H.-P. Haerri, G. E. Hall, P. L. Houston, I. Burak, and J. W. Hepburn, J. Chem. Soc. Frad. Trans. 2 **85**, 925 (1989).
[22]R. Ogorzalek Loo, H.-P. Haerri, G. E. Hall, and P. L. Houston, J. Chem. Phys. **90**, 4222 (1989).
[23]K. A. Trentelman, Ph.D. thesis, Cornell University, 1989.
[24]K. A. Trentelman, D. B. Moss, and P. L. Houston (in preparation).
[25]The data were smoothed to remove excessive noise since this transformation involves taking a derivative.
[26]M. J. S. Dewar, J. Am. Chem. Soc. **106**, 209 (1984).
[27]*CRC Handbook of Chemistry and Physics, 64th ed.* (CRC, Florida, 1983-84).
[28]M. Baba, I. Hanazaki, and U. Nagashima, J. Chem. Phys. **82**, 3938 (1985).
[29]H. Zuckermann, B. Schmitz, and Y. Haas, J. Phys. Chem. **92**, 4835 (1988).
[30]K. W. Watkins and W. M. Word, Int. J. Chem. Kinet. **6**, 855 (1974).
[31]R. Loudon, *The Quantum Theory of Light*, 2nd ed. (Oxford University, Oxford, 1983), p. 76.
[32]R. J. Campbell and E. W. Schlag, J. Am. Chem. Soc. **89**, 5103 (1967).
[33]G. S. Ondrey and R. Bersohn, J. Chem. Phys. **81**, 4517(1984).
[34]M. Kawasaki, H. Sato, H. Shinohara, and N. Nishi, Laser Chem. **7**, 109 (1987).
[35]G. E. Busch and K. R. Wilson, J. Chem. Phys. **56**, 3626 (1972).
[36]N. C. Baird and H. B. Kapthal, Can. J. Chem. **55**, 863 (1977); N. C. Baird, Pure Appl. Chem. **49**, 223 (1977).
[37]P. J. Robinson and K. A. Holbrook, *Unimolecular Reactions* (Wiley-Interscience, London, 1972).
[38]J. Solomon, C. Jonah, P. Chandra, and R. Bersohn, J. Chem. Phys. **55**, 1908 (1971).
[39]G. K. Chawla, G. C. McBane, P. L. Houston, and G. C. Schatz, J. Chem. Phys. **88**, 5481 (1988).
[40]G. C. McBane, S. H. Kable, and P. L. Houston (in preparation).

[41]In practice, the acceleration is determined from the delay time and the arrival time at the center of the distribution, where $v_z = 0$, so that for our mass spectrometer, the acceleration is given by $a_z = 46.60(t_{arr} - t_d)^{-2}$. Measuring the applied voltage directly is inaccurate because the extraction pulse is not a perfect square wave.